Science Advances
AAAS

advances.sciencemag.org/cgi/content/full/5/2/eaau6732/DC1

Supplementary Materials for

Tie2 activation promotes choriocapillary regeneration for alleviating neovascular age-related macular degeneration

Jaeryung Kim, Jang Ryul Park, Jeongwoon Choi, Intae Park, Yoonha Hwang, Hosung Bae, Yongjoo Kim, WooJhon Choi, Jee Myung Yang, Sangyeul Han, Tae-Young Chung, Pilhan Kim, Yoshiaki Kubota, Hellmut G. Augustin, Wang-Yuhl Oh*, Gou Young Koh*

*Corresponding author. Email: gykoh@kaist.ac.kr (G.Y.K.); woh1@kaist.ac.kr (W.-Y.O.)

Published 13 February 2019, *Sci. Adv.* **5**, eaau6732 (2019)
DOI: 10.1126/sciadv.aau6732

The PDF file includes:

Other Supplementary Material for this manuscript includes the following:

(available at advances.sciencemag.org/cgi/content/full/5/2/eaau6732/DC1)

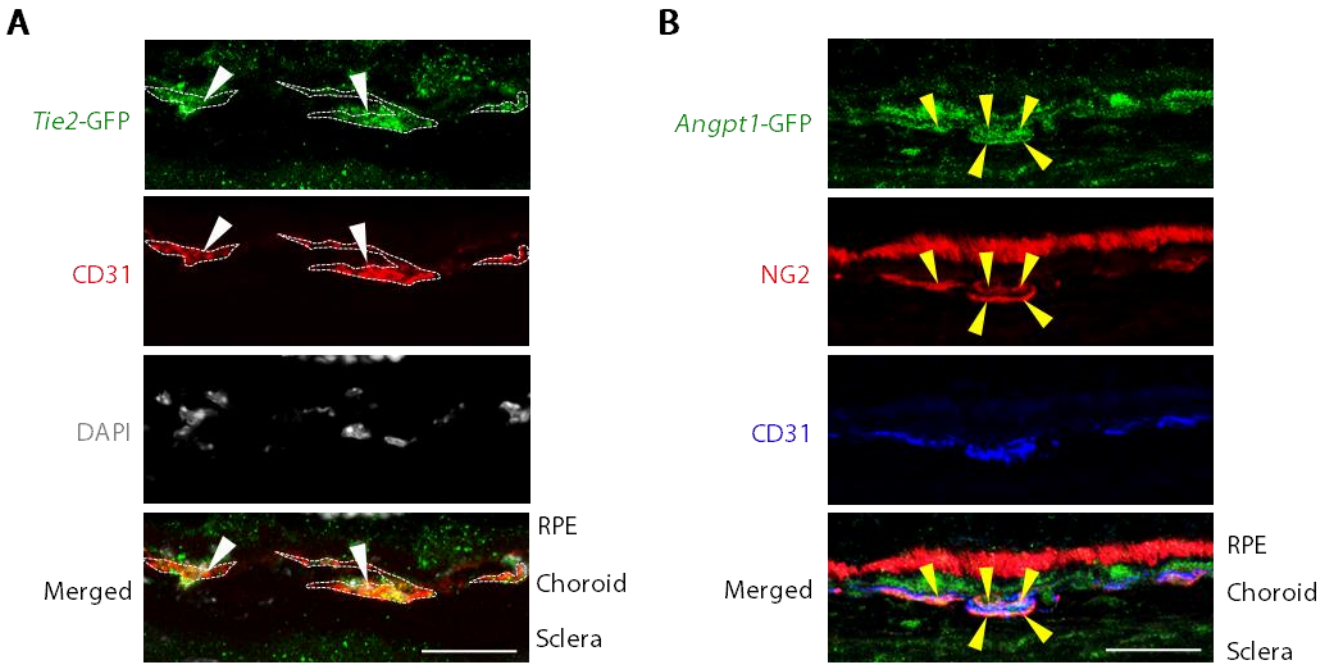

Fig. S1. Expressions of Tie2 and Angpt1 in the RPE-choroid complex. (**A**) Cross-sectional images of RPE-choroid complex of *Tie2*-GFP mouse. Note that GFP signals are detected in ECs of choroidal vessels (white arrowheads). Scale bar, 20 μm. Dashed lines demarcate the margins of choriocapillaris. (**B**) Cross-sectional images of RPE-choroid complex of *Angpt1*-GFP mouse. Note that GFP signals are detected in pericytes around choriocapillaris (yellow arrowheads). Scale bar, 20 μm.

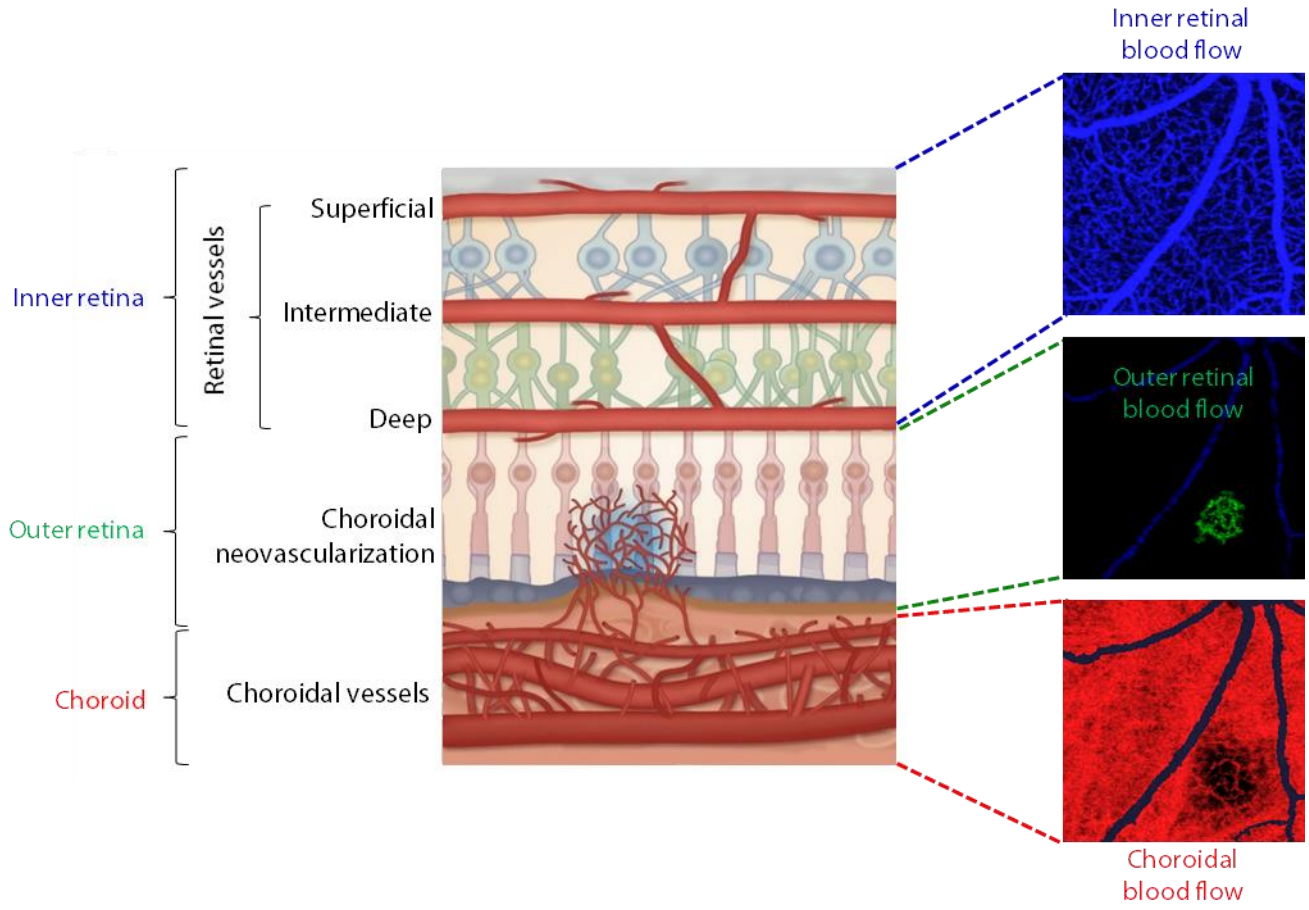

Fig. S2. Generation of en face OCT angiograms for measurement of retinal and choroidal blood flow. Schematic diagram defining inner retinal, outer retinal, and choroidal layers. *En face* OCT angiograms were visualized by separate projections of each flattened cross-sectional OCT angiogram in three depth ranges: inner retinal, outer retinal, and choroidal layers. The outer plexiform layer and Bruch's membrane are the boundaries separating inner retinal, outer retinal, and choroidal layers.

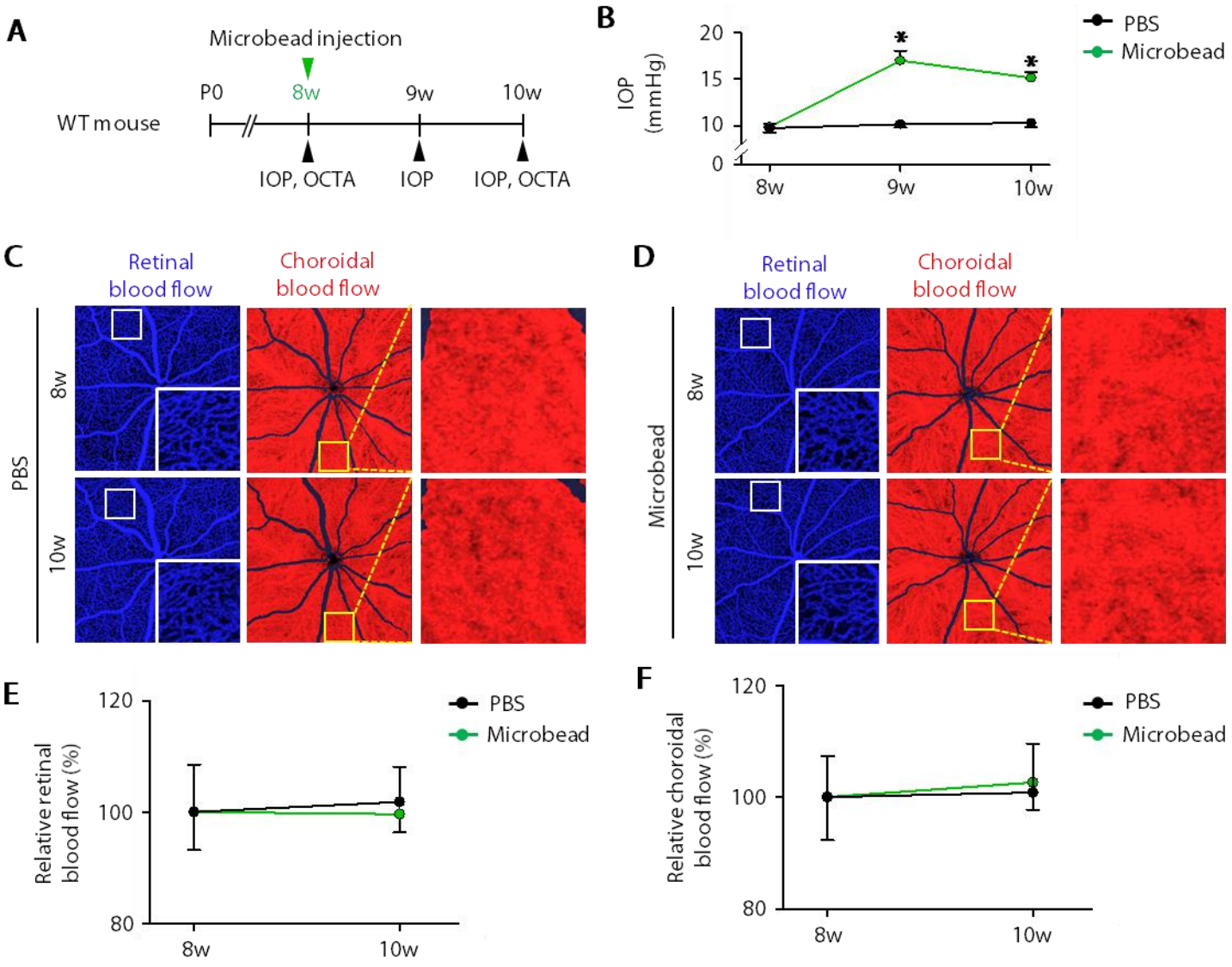

Fig. S3. Elevated IOP is not responsible for reduced choroidal blood flow. (**A**) Diagram depicting the experiment schedule of microbeads injection-induced ocular hypertension model in 8-week-old WT mice. Eyes were injected with 1 and 6 μm-sized microbeads in PBS (2 μl). (**B**) Temporal changes in IOP. (**C** and **D**) *En face* OCT angiograms showing retinal blood flow (left panels) and choroidal blood flow (middle panels) acquired by longitudinal OCTA imaging of eyes. Each area marked by a white box is magnified in the corner. Each area marked by a yellow box is magnified on the right panel. (**E** and **F**) Temporal changes in relative retinal (E) and choroidal (F) blood flow. Error bars represent mean ± s.d. Each group, n = 7. **P* < 0.05 vs. WT by Mann-Whitney *U* test.

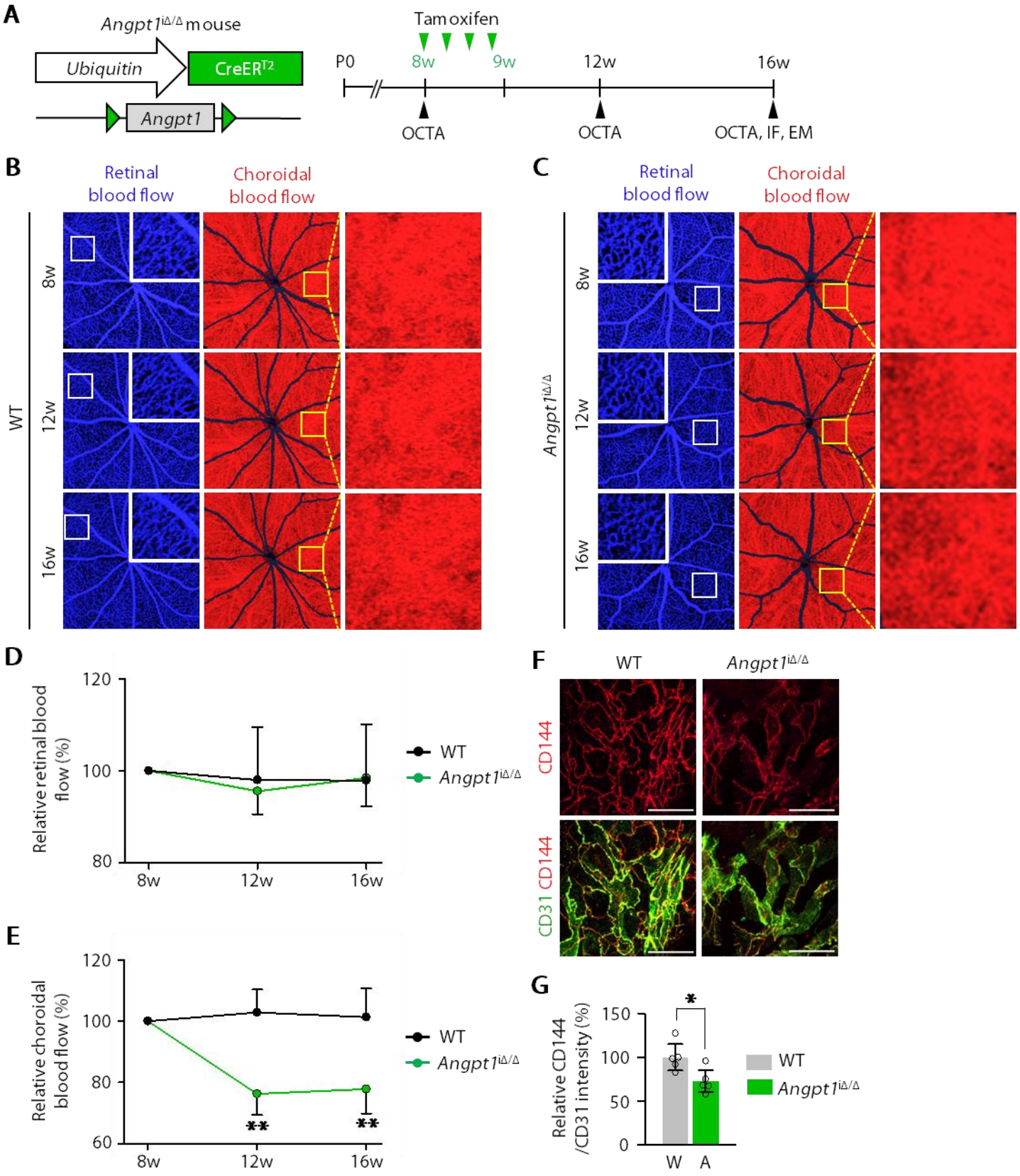
A
Angpt1iΔ/Δ mouse
Ubiquitin
CreERT2
Angpt1
Tamoxifen
P0
8w
9w
12w
16w
OCTA
OCTA
OCTA, IF, EM
B
Retinal blood flow
Choroidal blood flow
WT
8w
12w
16w
C
Retinal blood flow
Choroidal blood flow
Angpt1iΔ/Δ
8w
12w
16w
D
Relative retinal blood flow (%)
120
100
80
8w
12w
16w
WT
Angpt1iΔ/Δ
E
Relative choroidal blood flow (%)
120
100
80
60
8w
12w
16w
**
**
WT
Angpt1iΔ/Δ
F
WT
Angpt1iΔ/Δ
CD144
CD31 CD144
G
Relative CD144 /CD31 intensity (%)
150
100
50
0
*
W
A
WT
Angpt1iΔ/Δ

Fig. S4. Global *Angpt1* deletion in adult mice causes damage and loss of choriocapillaris. (**A**) Diagram of schedule for global depletion of *Angpt1* in 8-week-old mice and analyses at 8, 12, and 16 weeks of age using *Angpt1*$^{i\Delta/\Delta}$ mice. (**B** and **C**) *En face* OCT angiograms showing retinal blood flow (left panels) and choroidal blood flow (middle panels) acquired by longitudinal OCTA imaging of eyes. Each area marked by a white box is magnified in the corner. Each area marked by a yellow box is magnified on the right panel. (**D** and **E**) Temporal changes in relative retinal (D) and choroidal (E) blood flow. Error bars represent mean ± s.d. Each group, n = 10. $^{**}P < 0.005$ vs. WT by unpaired Student's *t*-test. (**F** and **G**) Images and comparison of CD144 intensity in CD31^{+} choriocapillaris. Error bars represent mean ± s.d. Each group, n = 5. $^{*}P < 0.05$ vs. WT by Mann-Whitney *U* test. Scale bars, 20 μm.

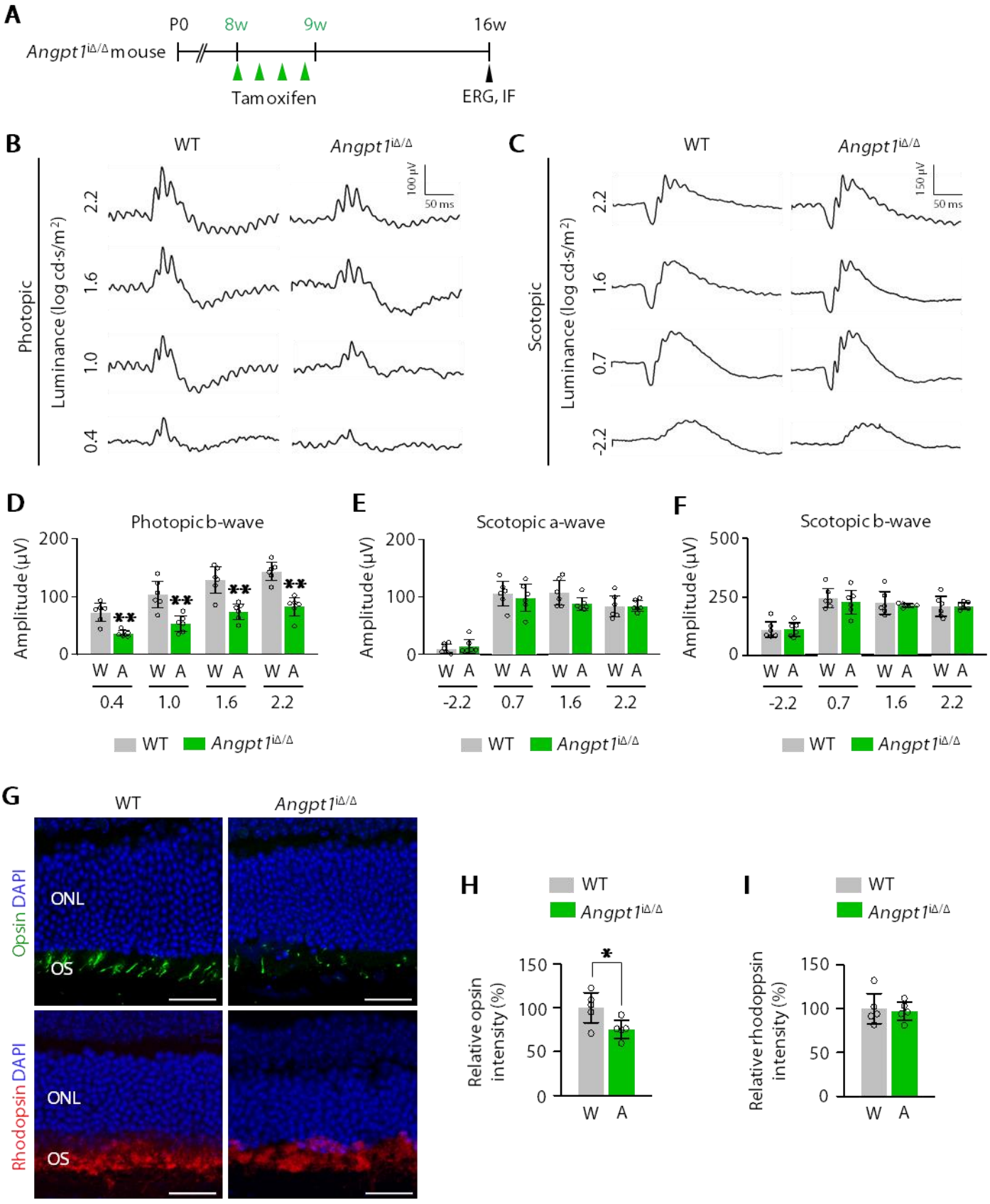
A
P0
8w
9w
16w
Angpt1iΔ/Δ mouse
Tamoxifen
ERG, IF
B
WT
Angpt1iΔ/Δ
Photopic
Luminance (log cd·s/m²)
2.2
1.6
1.0
0.4
100 μV
50 ms
C
WT
Angpt1iΔ/Δ
Scotopic
Luminance (log cd·s/m²)
2.2
1.6
0.7
-2.2
150 μV
50 ms
D
Photopic b-wave
Amplitude (μV)
200
100
0
W A W A W A W A
0.4 1.0 1.6 2.2
**
WT
Angpt1iΔ/Δ
E
Scotopic a-wave
Amplitude (μV)
200
100
0
W A W A W A W A
-2.2 0.7 1.6 2.2
WT
Angpt1iΔ/Δ
F
Scotopic b-wave
Amplitude (μV)
500
250
0
W A W A W A W A
-2.2 0.7 1.6 2.2
WT
Angpt1iΔ/Δ
G
WT
Angpt1iΔ/Δ
Opsin DAPI
ONL
OS
Rhodopsin DAPI
ONL
OS
H
WT
Angpt1iΔ/Δ
Relative opsin intensity (%)
150
100
50
0
*
W A
I
WT
Angpt1iΔ/Δ
Relative rhodoppsin intensity (%)
150
100
50
0
W A

Fig. S5. Loss of cone but not of rod photoreceptor in the eyes of global *Angpt1*-depleted mice. (**A**) Diagram for global depletion of *Angpt1* in 8-week-old mice and analyses 2 months later using *Angpt1*$^{i\Delta/\Delta}$ mice. (**B** and **C**) Representative wave responses of ERG in photopic (B) and scotopic (C) condition. (**D**) Comparisons of b-wave in photopic condition. Error bars represent mean ± s.d. Each group, n = 6. ***P* < 0.005 vs. WT by Mann-Whitney *U* test. (**E** and **F**) Comparisons of a- and b-wave amplitudes in scotopic condition. Error bars represent mean ± s.d. Each group, n = 6. (**G-I**) Expression of opsin and rhodopsin in photoreceptor layer. Error bars represent mean ± s.d. Each group, n = 6. **P* < 0.05 vs. WT by Mann-Whitney *U* test. Scale bars, 20 μm.

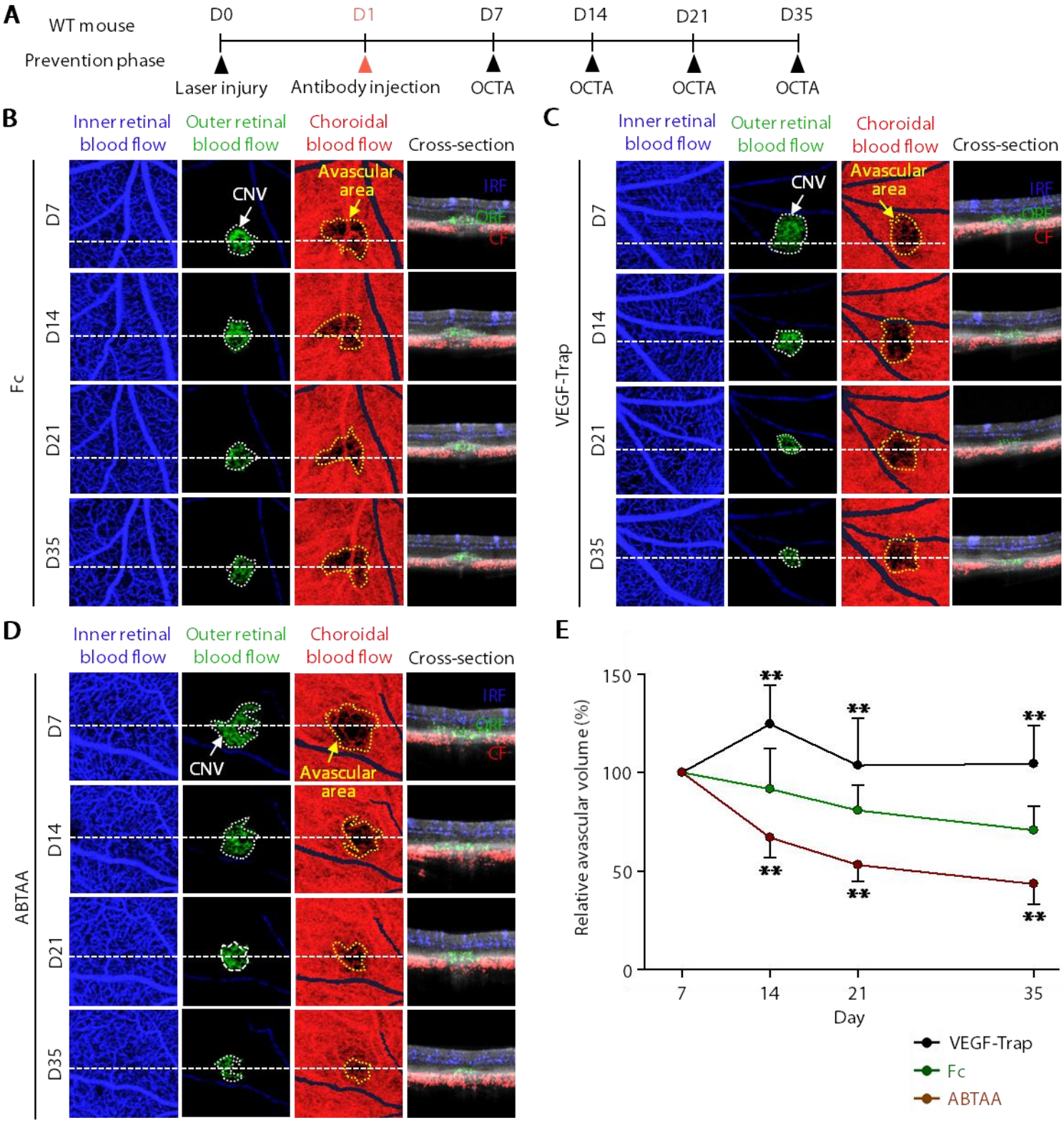
A
WT mouse
Prevention phase
D0
D1
D7
D14
D21
D35
Laser injury
Antibody injection
OCTA
OCTA
OCTA
OCTA
B
Inner retinal blood flow
Outer retinal blood flow
Choroidal blood flow
Cross-section
Fc
D7
D14
D21
D35
CNV
Avascular area
IRF
ORF
CF
C
VEGF-Trap
D
ABTAA
E
Relative avascular volume (%)
150
100
50
0
7
14
21
35
Day
VEGF-Trap
Fc
ABTAA
**

Fig. S6. ABTAA promotes regeneration of choriocapillaris surrounding the site of laser photocoagulation in the prevention phase. (**A**) Diagram of schedule for induction of CNV at D0, intravitreal administration of Fc, VEGF-Trap, or ABTAA (5 μg each) at D1, and intra-vital OCTA at D7, D14, D21, and D35 as a prevention phase. (**B**-**D**) *En face* OCT angiograms and selected cross-sectional OCT angiograms of the locations indicated by the white dotted lines showing inner retinal blood flow (blue), outer retinal blood flow (green), and choroidal blood flow (red) acquired by longitudinal OCTA imaging of eyes treated with Fc, VEGF-Trap, or ABTAA. *En face* angiogram of the outer retina showing the CNV (area demarcated by the white dotted boundary) and the choroid with avascular space (area demarcated by the yellow dotted boundary) surrounding the CNV. (**E**) Temporal changes in relative avascular volumes surrounding the site of laser photocoagulation. Error bars represent mean ± s.d. Each group, n = 13 to 17. $^{**}P < 0.005$ vs. Fc by one-way ANOVA followed by Student-Newman-Keuls post hoc test.

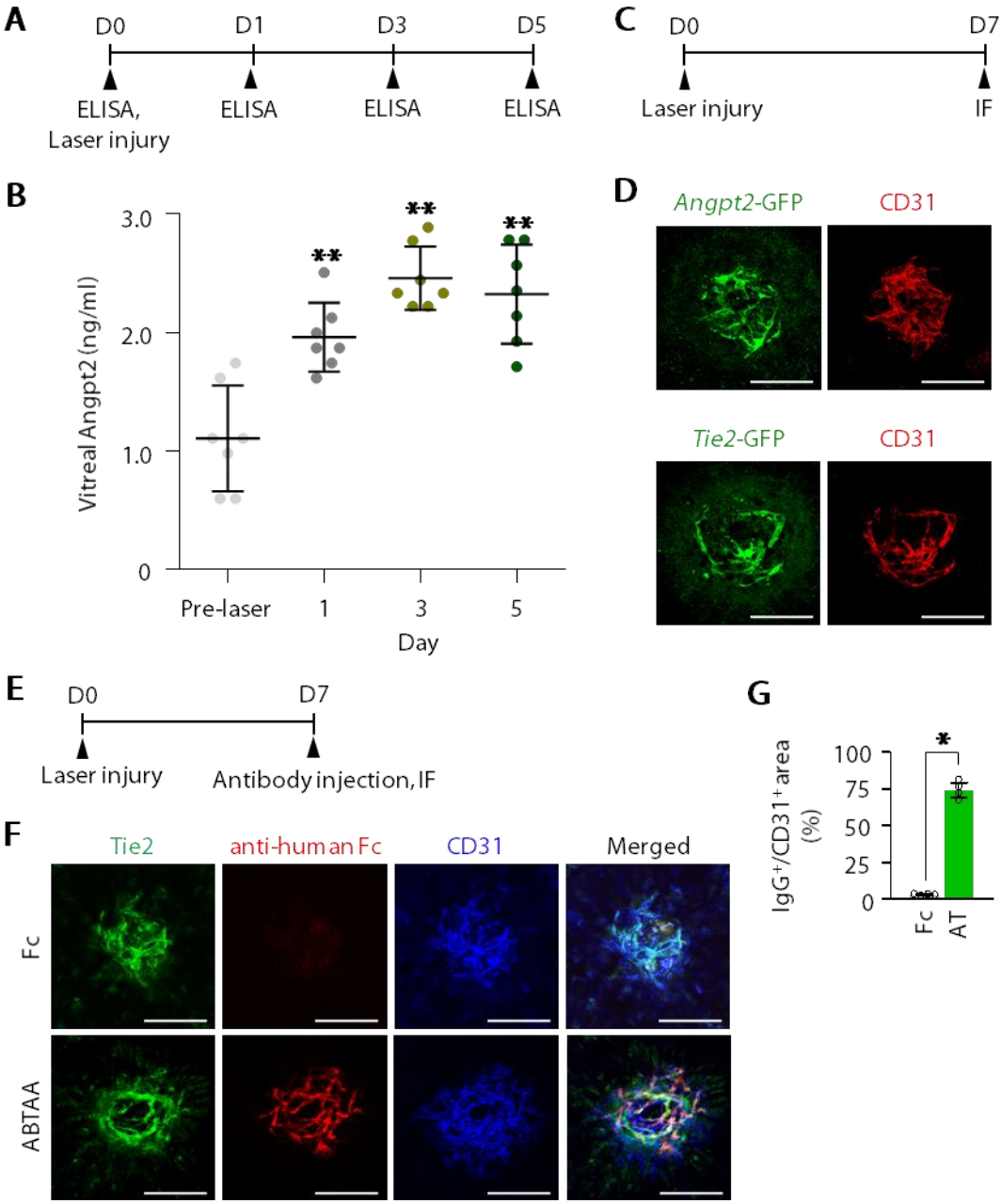

Fig. S7. ABTAA forms the Angpt2-Tie2-ABTAA complex in the mouse CNV model. (**A**) Diagram of schedule for induction of CNV at D0 and ELISA at pre-laser, D1, D3, and D5. (**B**) Comparison of temporal changes in vitreal Angpt2 level. Error bars represent mean ± s.d. Each group, n = 7. $^{**}P < 0.005$ vs Pre-laser by Mann-Whitney *U*-test. (**C**) Diagram of schedule for induction of CNV at D0 and IF staining at D7. (**D**) Representative images showing Angpt2^{+} or Tie2^{+} ECs of laser-induced CNV. Scale bars, 100 μm. (**E**) Diagram of schedule for induction of CNV at D0, intravitreal administration of Fc or ABTAA (5 μg each) at D7, and IF staining at 30 min after intravitreal administration. (**F** and **G**) Images and comparisons of expressions of Tie2 and CD31, and co-localization of Fc or ABTAA in ECs of CNV. Fc or ABTAA was directly detected with anti-human IgG antibody. Error bars represent mean ± s.d. Each group, n = 4. $^{*}P < 0.05$ by Mann-Whitney *U*-test. AT, ABTAA. Scale bars, 100 μm.

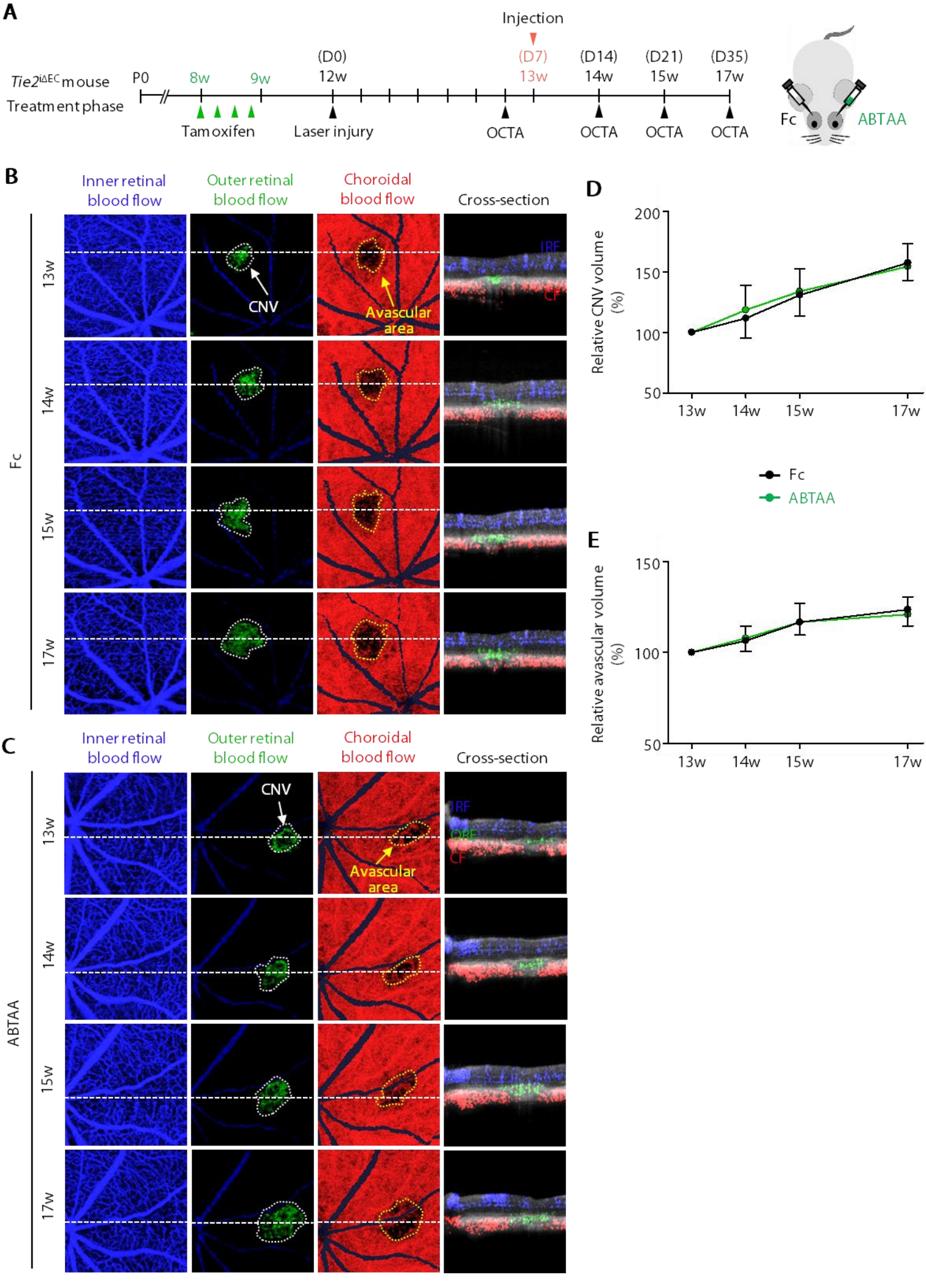
A
Injection
(D0)
(D7)
(D14)
(D21)
(D35)
Tie2iΔEC mouse
Treatment phase
P0
8w
9w
12w
13w
14w
15w
17w
Tamoxifen
Laser injury
OCTA
OCTA
OCTA
OCTA
Fc
ABTAA
B
Inner retinal blood flow
Outer retinal blood flow
Choroidal blood flow
Cross-section
Fc
13w
14w
15w
17w
CNV
Avascular area
IRF
CF
C
ABTAA
ORF
D
Relative CNV volume (%)
200
150
100
50
13w
14w
15w
17w
Fc
ABTAA
E
Relative avascular volume (%)
150
100
50

Fig. S8. Analyses of the effects of ABTAA treatment in adult *Tie2*-depleted mice. (**A**) Diagram of schedule for EC-specific depletion of *Tie2* in 8-week-old mice, induction of CNV after 4 weeks (D0), intravitreal administration of Fc or ABTAA (5 μg each) at D7, and intra-vital OCTA at D6, D14, D21 and D35 using $Tie2^{i\Delta EC}$ mice. (**B** and **C**) *En face* OCT angiograms and selected cross-sectional OCT angiograms of the locations indicated by the white dotted lines showing inner retinal blood flow (blue), outer retinal blood flow (green), and choroidal blood flow (red) acquired by longitudinal OCTA imaging of eyes. (**D** and **E**) Temporal changes in relative CNV volume (D) and avascular volume surrounding the site of laser photocoagulation (E). Error bars represent mean ± s.d. Each group, n = 11 to 12.

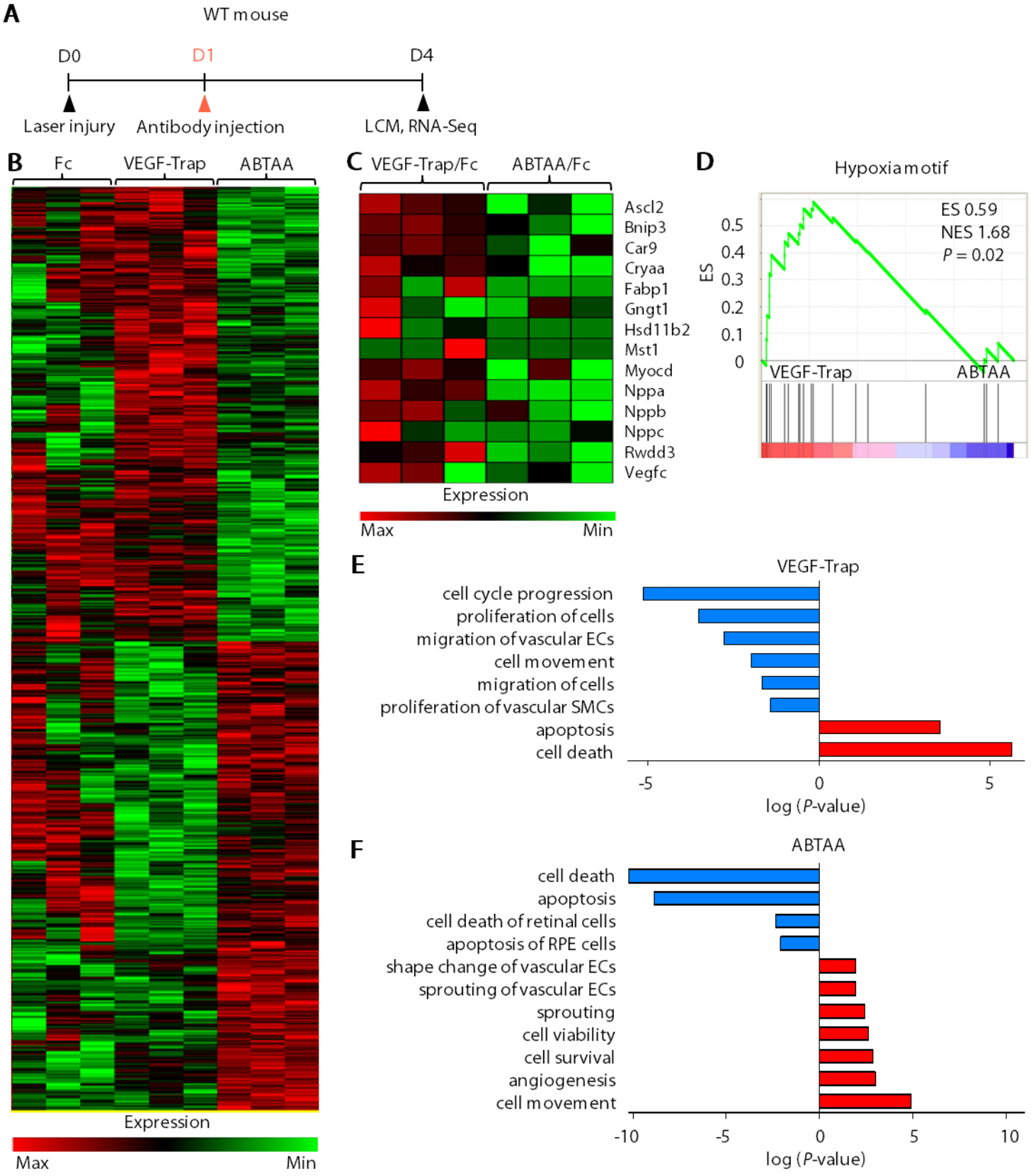
A
WT mouse
D0
D1
D4
Laser injury
Antibody injection
LCM, RNA-Seq
B
Fc
VEGF-Trap
ABTAA
Expression
Max
Min
C
VEGF-Trap/Fc
ABTAA/Fc
Ascl2
Bnip3
Car9
Cryaa
Fabp1
Gngt1
Hsd11b2
Mst1
Myocd
Nppa
Nppb
Nppc
Rwdd3
Vegfc
Expression
Max
Min
D
Hypoxia motif
ES
0.5
0.4
0.3
0.2
0.1
0
ES 0.59
NES 1.68
P = 0.02
VEGF-Trap
ABTAA
E
VEGF-Trap
cell cycle progression
proliferation of cells
migration of vascular ECs
cell movement
migration of cells
proliferation of vascular SMCs
apoptosis
cell death
-5
0
5
log (P-value)
F
ABTAA
cell death
apoptosis
cell death of retinal cells
apoptosis of RPE cells
shape change of vascular ECs
sprouting of vascular ECs
sprouting
cell viability
cell survival
angiogenesis
cell movement
-10
-5
0
5
10
log (P-value)

Fig. S9. RNA-seq analysis of CNV lesions and surrounding tissues treated with VEGF-Trap and ABTAA. (**A**) Diagram of schedule for induction of CNV at D0, intravitreal administration of Fc, VEGF-Trap, or ABTAA (5 μg each) at D1, and their analyses at D4. (**B**) RNA-Seq gene expression heatmap of DEGs ($P < 0.05$) between VEGF-Trap- and ABTAA-treated groups. (**C**) Heatmap of hypoxia signature genes upregulated by VEGF-Trap but downregulated by ABTAA relative to Fc. (**D**) GSEA of hypoxia-responsive gene set in VEGF-Trap- or ABTAA-treated groups. ES, enrichment score; NES, normalized enrichment score. (**E** and **F**) Representative disease and biological functional terms of DEGs in VEGF-Trap or ABTAA group. Ranks were ordered according to their *P* value of Fisher's Exact test, and determined for their activation or inhibition by activation z-score. LCM, laser capture microdissection. See table S1 for details.

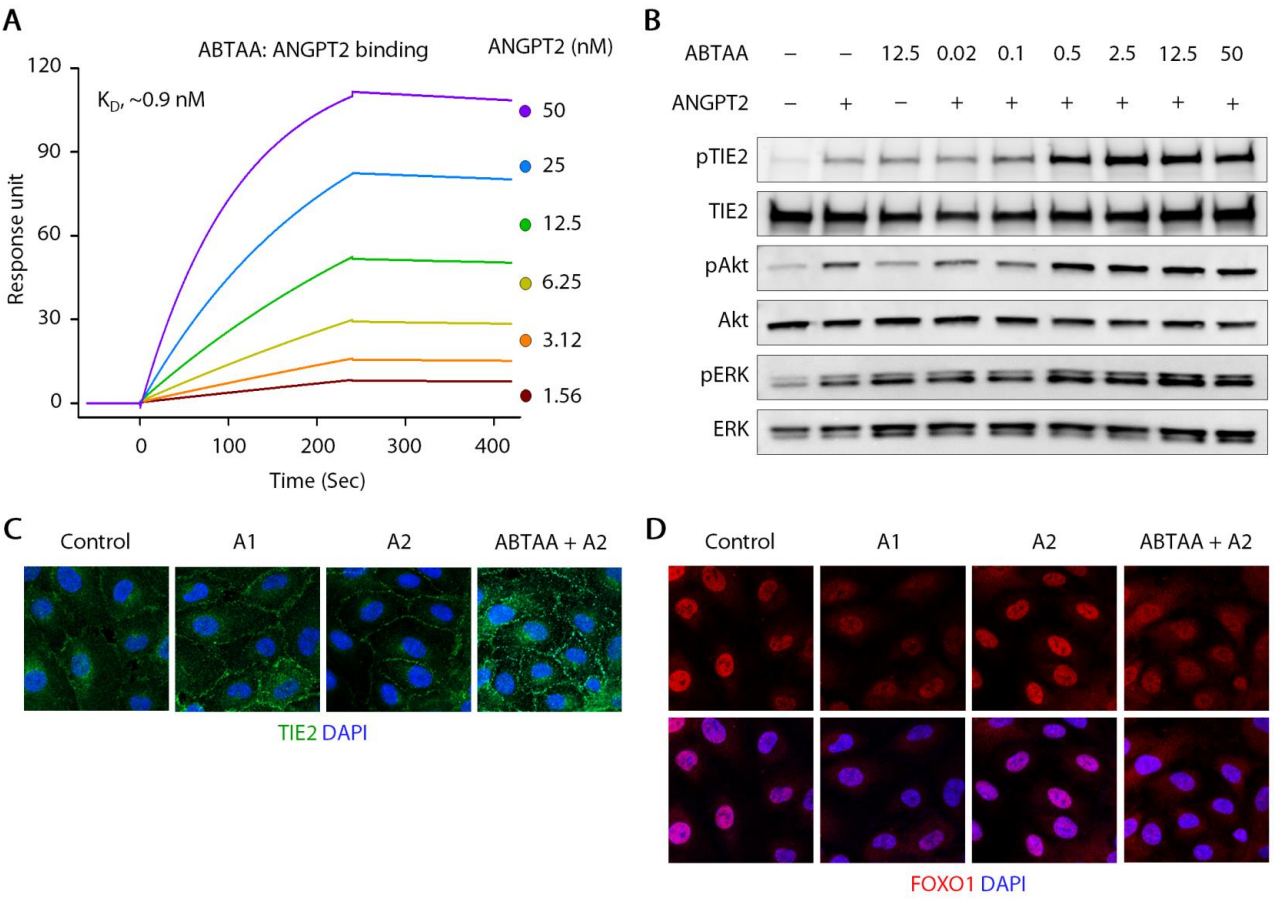

Fig. S10. ABTAA binds to ANGPT2 and activates TIE2 and its downstream effectors. (**A**) Representative dose-response surface plasmon resonance sensograms of ANGPT2 binding to immobilized ABTAA. ANGPT2 concentrations in each injection are indicated by different colors. (**B-D**) Serum-starved confluent HUVECs were treated with either ANGPT2 (A2, 1 μg/ml) or COMP-Angpt1 (A1, 0.5 μg/ml) with or without ABTAA for 30 min. (B) Immunoblot detection of TIE2, pTIE2, and its downstream signaling proteins Akt, pAkt, ERK, and pERK in serum-starved HUVECs that were treated with human ANGPT2 with or without ABTAA (0.02, 0.1, 0.5, 2.5, 12.5, and 50 μg/ml). (C) Confocal images showing that ABTAA induces TIE2 translocation to cell-cell contacts. Scale bars, 20 μm. (D) ABTAA-induced nuclear clearance of FOXO1. Scale bars, 20 μm.